DIELECTRIC CHARACTERIZATION OF THE YEAST CELL BUDDING CYCLE

José L. Sebastián Franco[1, *], Aránzazu Sanchis Otero[2], José Roldan Madroñero[3], and Sagrario M. San Martin[1]

[1]Dpto Física Aplicada III, Facultad de Físicas, Universidad Complutense Madrid, Spain

[2]Centro Nacional de Sanidad Ambiental, Instituto de Salud Carlos III, Majadahonda, Spain

[3]Servicio de Radioprotección, Instituto de Salud Carlos III, Majadahonda, Spain

Abstract—We combine experimental electrorotation data and the numerical analysis of the electrorotation chamber and cell to electrically characterize the *Saccharomyces cerevisiae* yeast budding cell cycle and to obtain the electrical parameters of the cell. To model the yeast cell we use spherical and doublet-shaped geometries with a four layered structure: cytoplasm, membrane, inner and outer walls. To derive the geometrical and electrical parameters of the yeast model we use the finite element method to calculate the yeast rotational velocity spectrum and apply the least-square method to fit the calculated values to experimental data. We show that the calculated yeast electrorotation spectra undergo significant changes throughout its budding cycle and that the calculated spectra fit experimental data obtained for 0% (start) and 50% representative budding stages very well. The analysis also shows the small variation of the rotation crossover frequency within a full span of the yeast growth cycle. As an application of this work, we apply the Maxwell-Wagner formalism to obtain the dielectric spectra of truly synchronized yeast suspensions.

* Corresponding author: Jose Luis Sebastian Franco (jlsf@fis.ucm.es).

1. INTRODUCTION

Yeasts are unicellular eukaryotes which are widely used in several biotechnological processes that include brewing and the production of a variety of biochemical compounds. Techniques using electric fields for hybridization and the production of transgenic yeast strains have promoted the dielectric characterization of yeasts as an active and continuously expanding field of research [1, 2] leading to practical and commercial applications. For the experimental characterization of individual cells, non-invasive AC electrokinetic techniques such as electrorotation (ER), dielectrophoresis (DEP) and electroorientation (EO) are used, whereas for biological cell suspensions the dielectric spectroscopy (DS) technique is generally applied [3–6]. The geometrical dimensions, conductivity and permittivity of the main compartments of cells in suspension are obtained by combining theoretical modeling and DS. However, analytical methods can only be applied to very simple geometrical cell shapes. Thus, numerical techniques such as the finite element (FEM) [7, 8] or the boundary element methods (BEM) [9–11] are used to determine the electric properties of both single-cell and cell suspensions with a realistic cell geometry and structure.

The yeast *Saccharomyces cerevisiae* is of particular interest, as characterization of its life cycle provides a good knowledge about the molecular mechanisms that determine cell specialization, control of gene expression in eukaryotes and for addressing numerous problems in cell biology [12, 13]. The *S. cerevisiae*, experiences a pattern of growth and division called budding. The budding yeast cells are doublet-shaped, i.e., mother and daughter (bud) cells are connected by a junction, which becomes narrower and is closed during septum formation in cell division. The *S. cerevisiae* is the yeast commonly used in brewery industry and therefore, real-time monitoring of the dynamic behavior of cell growth in suspensions is of primary interest [14, 15]. The monitoring provides integrated information on yeast cell concentration, changes in cell volume as well as shape and cell viability. The experimental simplicity of the dielectric spectroscopy (DS) has promoted as preferred technique for the electrical characterization of cell suspensions and thus, it has been applied to study the behavior of yeast cell cultures in different budding states [16–18]. To explain the experimentally observed changes in DS, different dielectric effective medium approaches, based on the formulas of Maxwell, Looyenga or Hanai [19, 20] and on the single (multi-)shell particle model [21] have been applied. As a general procedure, the suspension with spherical yeasts is considered to be synchronous

and the dielectric characterization is obtained by fitting the well-known equation for the complex permittivity with various Cole-Cole relaxation terms [22] to experimental dielectric spectra.

However, all the theoretical models used to interpret DS experimental results are only valid for low concentrations, contrary to the high concentrations required in high sensitivity measurements of permittivity of suspensions. This severe limitation has confined most practical applications of dielectric spectroscopy on yeast suspensions to biomass monitoring.

Contrary to DS systems, experimental single-cell electrorotation chambers are very complex and need to be carefully characterized to ensure the validity and accuracy of the measurements [23–25]. However, the ER technique has the advantage of removing the concentration limitation as well as the uncertainties arising from non-uniformity in the structure of the cells in suspension. An electrorotation spectrum is obtained by determining, as a function of the frequency of the applied field, the rate and sense of rotation of particles produced by the torque induced by the rotating field. Analyses of such spectra can be used to derive the dielectric properties of the various compartments of cells. In addition, the theoretical analysis of ER does not need to take into account electrical interactions between cells.

In this paper, we present the dielectric characterization of a complete cell growth cycle of a single *S. cerevisiae* budding yeast, from "start" to cell separation. For this, we setup an ER chamber and compare the budding yeast experimental rotational velocity data with calculated spectra obtained from the numerical analysis of the cell-chamber system. For the theoretical analysis we use the finite element method, and at every budding state we use a nonhomogeneous, multilayered cell model that realistically represents the doublet-shaped yeast. To assess the effect of forces and torques acting on the yeast under typical experimental conditions, we characterized the nonuniform rotating fields in the ER chamber and determine the square and the gradient of the square of the electric field. To determine the high number of independently accessible electrical and geometrical parameters imposed by the complexity of the model used in the analysis, we measure and calculate electrorotation spectra for different stages of yeast growth and environmental conditions. As an application of this work, we obtain the dielectric spectra of synchronized suspensions of yeasts derived as part of the Maxwell-Wagner formalism.

Although ER has been used extensively in the literature, it has been mostly applied to single-shell spherical or spheroidal particles

in slightly nonuniform rotating electric fields [26, 27], and to our knowledge, not much experimental work appears to assess the influence of torque on doublet-shaped yeast particles under typical experimental conditions.

The layout of the paper is as follows. In Section 2 we first describe the experimental ER chamber and analyze the field distribution within the chamber by calculating the squared electric field and its gradient. Then we present our realistic yeast model, and we determine the electric field distribution within the cell, its complex polarizability and torque using the FEM method. As a test of our results, we compare the numerical values for the torque on the realistic cell model with the values given by the analytical solution for a homogeneous spherical yeast with an equivalent permittivity. In Section 3 we present the results for both calculated and measured rotational velocity spectra at different yeast budding states and for different conductivities of the suspending medium. We derive the electrical and geometrical parameters of each compartment of the yeast cell by fitting the calculated spectra to the experimental rotational data. Once we have characterized the single budding yeast, we apply the calculated cell parameters to the Maxwell-Wagner formalism to obtain the dielectric spectra of synchronized cell solutions of different concentrations. We discuss our conclusions in Section 4.

2. ELECTROROTATION CHAMBER AND CELL MODEL

2.1. Experimental Electrorotation Chamber

Amongst the various designs of chambers with different electrode configurations and correction factors for the field strength that are available in the literature, we choose a planar four-rounded tip microelectrode configuration as it reduces the torque deviations that would be experienced by a spherical object at different radii from the center of the chip [25]. The semicircular electrodes of $\delta = 100\,\mu\text{m}$ of diameter spaced $\delta = 100\,\mu\text{m}$ between opposite structures are arranged on top of diced glass wafers of $12 \times 12\,\text{mm}$ and $1.5\,\text{mm}$ of thickness. The electrode chip is mounted on a drilled PCB with the microstrip lines needed for electrical connection to the quadrature signal generator. The pads of the electrodes on the glass are soldered to the internal edge (close to the hole) of microstrip lines of the PCB. In the experimental chamber shown in Fig. 1(a), the PCB is held on a methacrylate platform housed above the stage of an optical microscope (Axio Examiner A.1, Karl Zeiss) equipped with a video camera (CR450x2 Optronis) connected to a PC for experimental observation and image capture. The response of the cell to a rotating

(a)   (b)
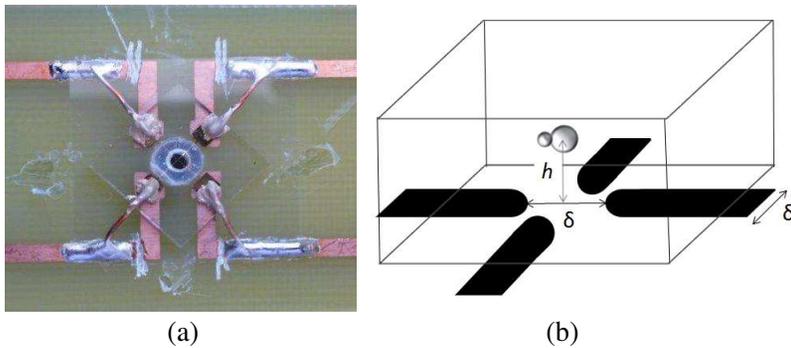
Figure 1. Experimental and simulated model of the electrorotation chamber with four semicircular electrodes of diameter and gap $\delta = 100\,\mu\text{m}$ on the base. The figure also shows a budding yeast (not to scale) placed at a height h above the electrode plane.

voltage signal of $1.5V_{pp}$ and frequency within the range from $4\,\text{kHz}$ to $40\,\text{MHz}$ was assessed at five points per decade. A saline solution was prepared by addition of $20\,\text{mM}$ KCl to DI water to adjust the conductivity of the suspending medium to the desired value. For the measurement of the conductivity we used a Mettler Toledo FiveEasy conductivity meter. Depending on the cell concentration, 10 or $20\,\mu\text{l}$ of stock suspension were added to the saline solution to get the sample for experimentation. A volume of $10\,\mu\text{l}$ of this sample was pipetted in a reusable and adhesive silicone well located over the electrodes and covered lately by a coverlid for avoiding evaporation and contamination of the sample. The image analysis of the electrorotation of the yeast cell was performed using ImageJ, a public domain Java-based image processing program. Cell dimensions are obtained through the edition of the corresponding recorded video frames, and rotational spectra of individual cells through a plugin command developed for the purpose, where the rotation rate at each frequency is extracted after images treatment and processing. The average of five complete rotation cycles with five points per decade lead to the rotational spectra of the analyzed individual cell.

2.2. Numerical Analysis of the Chamber Field Distribution

When subjected to an AC rotating electric field, the yeast is polarized and has an induced dipole moment. The rotating field creates a torque that directly affects the cell with the induced dipole moment. Because the rotation rate depends directly on the square of the electric field strength, we need to have a good knowledge of the electric field
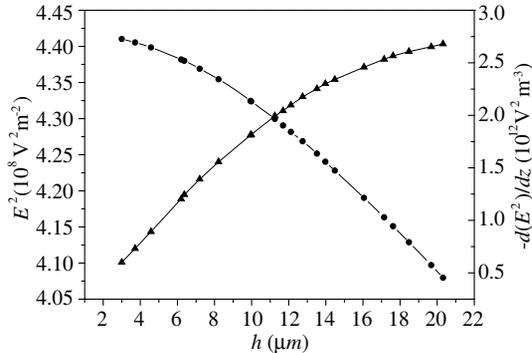
Figure 2. Squared electric field (circles) and (minus) its gradient (up triangles) along the vertical axis in the chamber as a function of the height h. The chamber is filled with a suspending medium with $\varepsilon_{rext} = 80$ and $\sigma_{ext} = 0.1\,\mathrm{S/m}$. The frequency is $1\,\mathrm{MHz}$.

distribution within the chamber. For this, we first numerically analyze the experimental chamber with the four rounded-tip electrodes, as shown in Fig. 1(b). With the chamber filled of suspending medium with complex permittivity $\tilde{\varepsilon}_{ext}$ but without the cell, we solve the Laplace equation by using the adaptive-mesh finite-element software COMSOL Multiphysics. To generate the rotating field, the electrodes are driven by the same voltages used in the experimental setup, i.e., four sinusoidal voltages of equal amplitude $V = 1.5V_{pp}$ successively phase-shifted by $\pi/2$ [28]. We study the frequency range from $4\,\mathrm{kHz}$ to $1\,\mathrm{GHz}$ and assume that the electrode response is linear and that electrode polarization effects are negligibly small. In addition, we do not consider in our calculations the influence of the gradient of the phase of the electric field on the force and torque, which could produce traveling wave effects [29].

The squared electric field and (minus) its gradient responsible for the torque and force acting on the particle respectively, along the vertical axis as a function of h at the frequency of $1\,\mathrm{MHz}$ are shown in Fig. 2.

Figure 2 gives a first indication to understand the physical behavior of the system, because we recall that in the dipole approximation [cf. Eq. (2)], and momentarily ignoring the effect of the particle on the field, the torque is essentially the imaginary part of the particle effective polarizability times the magnitude shown in Fig. 2.

2.3. Yeast Cells Culture

Strain BY4741 of *S. cerevisiae* was donated by the Department of Microbiology II of the Faculty of Pharmacy of the UCM. Cultures were maintained and grown up at the Service of Mycology of the National Centre of Microbiology of the Institute of Health Carlos III (ISCIII). The cells were cultured in Sabouraud Dextrose broth (Becton and Dickinson Company, USA) at 30°C, harvested after 24 hours and washed in distilled DI water three times. The stock sample was kept in DI water, with a cell density $\sim 10^5$–10^6 cells/ml.

2.4. Yeast Cell Model

Although spherical single and double-shell models have been the most commonly yeast models used for theoretical calculations, in this work we use a spherical four-shelled model, shown in Fig. 3(a), consisting of cytoplasm, membrane and inner and outer walls. This cell structure best fits the experimental ER spectra and electron micrographs of *S. cerevisiae* [30–33]. We consider five different doublet-shaped models for the cell growth cycle, with the same structure but with the volume of the spherical bud according to the corresponding stage developed from the initial spherical shape to the last one, namely 0%, 25%, 50%, 75% and 100% as shown in Fig. 3(b). In the analysis, the neck radius of the bud is kept constant until the bud becomes the same size as the initial cell. Finally, the bud separates from the mother cell to be the daughter cell [34].
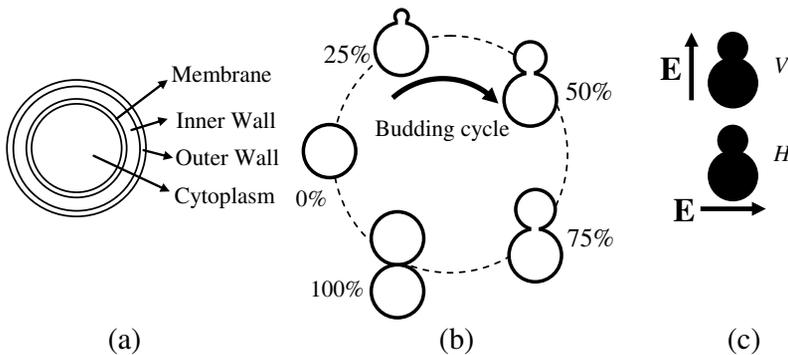
Figure 3. Structure and yeast shape models analyzed in the cell division cycle, (a) start stage 0%, (b) budding cycle and (c) horizontal and vertical orientations of the external applied electric field.

2.5. Polarizability and Rotational Velocity of the Yeast Cell

As first use of the yeast model we calculate its complex effective polarizability $\tilde{\alpha}_{eff}$, which gives the relation between the inducing external field at the center of the cell $\tilde{\mathbf{E}}_0$ and the effective induced dipole moment. The authors have already performed a detailed study on the polarizability and electromechanical effects on multilayered cells in nonuniform rotating fields [35] where we showed that the effective polarizability of a particle consisting of N layers and immersed in a suspending medium of complex permittivity $\tilde{\varepsilon}_{ext} = \varepsilon_{ext} - i\sigma_{ext}/\omega$ can be determined by the equation

$$\tilde{\alpha}_{eff}\tilde{\mathbf{E}}_0 = \frac{\text{Re}(\tilde{\varepsilon}_{ext})}{\tilde{\varepsilon}_{ext}} \sum_{i=1}^{N} \int_{V_i} (\tilde{\varepsilon}_i - \tilde{\varepsilon}_{ext})\tilde{\mathbf{E}}_i dV_i \tag{1}$$

where $\tilde{\varepsilon}_i$, $\tilde{\mathbf{E}}_i$, and dV_i denote the complex permittivity, electric field distribution, and volume element of the ith particle compartment, respectively. Eq. (1) is applicable to any cell structure with any geometric shape. We note that the yeast, considered as a rotating body, have anisotropic polarization, i.e., the effective permittivity of the cell depends on the orientation of the cell with respect to the direction of the applied electric field. Therefore, in the analysis we consider the horizontal (H) and vertical (V) orientations of the rotational axis of the cell to the applied electric field direction, as shown in Fig. 3(c), and we calculate the polarizabilities $\tilde{\alpha}_{eff\,H,V}$ by following the numerical procedure outlined in Ref. [36].

In this work, we will only consider the first-order dipolar forces and torques. For a detailed analysis of the influence of all the higher order multipolar terms induced in the cell by the nonuniform fields we refer the reader to Ref. [35]. The electrorotational torque is proportional to the out-of-phase part of the induced dipole moment and to the time-averaged applied electric field [37,38]. The expression of the torque can be found, e.g., in Ref. [39] and reads

$$\mathbf{N} = \frac{1}{2}\text{Re}\left(\tilde{\mathbf{p}}_{eff} x \tilde{\mathbf{E}}_0\right) = -\frac{1}{2}\text{Im}\left(\tilde{\alpha}_{eff}\right) E_0^2 \mathbf{e}_z \tag{2}$$

We can calculate the electrorotational torque acting on the cell by simply substituting in Eq. (2) the value of $\tilde{\alpha}_{eff}$ derived from Eq. (1). To test this approach, we recall the analytical expression for the torque that is available for an equivalent homogeneous spherical particle and compare our numerical results with the analytical values. For a spherical particle of radius R with complex permittivity $\tilde{\varepsilon}_{eq}$ and polarizability $\tilde{\alpha}_{eq}$ the torque is given by [35,40]

$$\mathbf{N} = 2\pi R^3 \text{Re}(\tilde{\varepsilon}_{ext})\text{Im}(f_{CM})E_0^2 \mathbf{e}_z \tag{3}$$

where f_{CM} is the Clausius-Mossotti factor [39]. To obtain the equivalent permittivity for our realistic four layer spherical yeast, we follow the classical method of smeared-out sphere [41]. In Section 3 we show that $\mathrm{Im}(\tilde{\alpha}_{eq}) = -4\pi R^3 \mathrm{Re}(\tilde{\varepsilon}_{\mathrm{ext}})\mathrm{Im}(f_{CM})$ and that the analytical results are in excellent agreement with the numerical simulation. This test for the 0% start budding allows us to apply Eq. (2) to the rest of doublet-shaped yeasts in the cell division cycle. The $\tilde{\alpha}_{eff}$ approach has the advantage that although there is no analytical expression for the rotational velocity of doublet particles, we can still fit our numerical results to experimental rotational data if we consider that the frequency dependent rotation velocity $\Omega(f)$ may be written as [42]

$$\Omega(f) = -F\mathrm{Im}\left(\tilde{\alpha}_{effH} + \tilde{\alpha}_{effV}\right)E_0^2 \qquad (4)$$

where $\tilde{\alpha}_{effH}$ and $\tilde{\alpha}_{effV}$ are the complex effective polarizabilities of the particle for the horizontal and vertical orientations of the electric field, and F is an adjustable parameter which is a function of the dynamic viscosity η and a form factor. We note that Eq. (4) averages the contribution of both field components for an arbitrary cell orientation. For spherical cells Eq. (4) can be written as

$$\Omega(f) = -2F\mathrm{Im}(\tilde{\alpha}_{eff})E_0^2 = -F \cdot 8\pi E_0^2 R^3 \mathrm{Re}(\varepsilon_{\mathrm{ext}})\mathrm{Im}(f_{CM}) \qquad (5)$$

The torque for a rotating sphere in a viscous fluid under laminar regime conditions is given by

$$N = 8\pi\eta R^3\Omega \qquad (6)$$

and the rotational velocity is then

$$\begin{aligned}\Omega(f) &= \frac{N}{8\pi\eta R^3} = \frac{4\pi R^3 \mathrm{Re}(\varepsilon_{\mathrm{ext}})\mathrm{Im}(f_{CM})E_0^2}{8\pi\,\eta R^3} \\ &= \frac{\mathrm{Re}(\varepsilon_{\mathrm{ext}})\mathrm{Im}(f_{CM})E_0^2}{2\,\eta}\end{aligned} \qquad (7)$$

We obtain the parameter F for the sphere from Eqs. (5) and (7) as

$$F = \frac{1}{16\,\pi\eta R^3} \qquad (8)$$

To derive the geometrical and electrical parameters of our yeast model we first assign initial $\tilde{\varepsilon}_i$, R_i values to the cell model, apply the external field $\tilde{\mathbf{E}}_0$, calculate numerically the fields $\tilde{\mathbf{E}}_i$, perform the integration in Eq. (1) and obtain the complex polarizabilities $\tilde{\alpha}_{effH}$ and $\tilde{\alpha}_{effV}$, the torque $\mathbf{N}$ and rotation velocity Ω. We then fit the numerical rotational velocity spectrum to experimental data across the frequency range from $4\,\mathrm{kHz}$ to $40\,\mathrm{MHz}$ by applying the least-square method with Mathematica. For fitting the spectra to data, we use the F as

adjustable parameter. The process is then repeated with modified
initial values $\tilde{\varepsilon}_i$, R_i until the best fit is obtained.

To reduce the computer hardware requirements and shorten
computing time, we assigned fixed values to some cell parameters.
These values were carefully selected among the experimental data
available in the literature. In particular, the thicknesses of the thick
and thin cell walls and the radius of the cytoplasm were taken from
published data of scanning (SEM) and transmission (TEM) electron
micrographs [43–47], and the value for the very low conductivity of the
membrane was fixed to be 10^{-7} S/m [48]. In addition, we have assumed
that the suspending medium does not exhibit a dielectric dispersion
so that $\mathrm{Re}(\tilde{\varepsilon}_{r\mathrm{ext}}) = 80$ remains fixed, but we perform the study for
different conductivity values σ_{ext}. In next section we present the
numerical values that we have obtained for the structure and dielectric
properties of the budding yeast.

3. RESULTS

We have obtained multiple both experimental and numerical rotational
spectra for different combinations of budding states and conductivities
of the suspending medium. To simplify the presentation of the results,
we have selected the analysis for two representative budding states: 0%
and 50% with spherical and doublet-shaped cell models respectively.
The results are presented for three characteristic values (0.001, 0.01
and 0.1 S/m) of the suspending medium conductivity σ_{ext}, over a broad
range of frequencies (10 kHz to 1 GHz).

For the calculations, the cell used in this study is always placed
on the vertical symmetry axis of the chamber with the cell center at
height $h = 4\,\mu$m above the electrode plane. We determined this height

Table 1. Values for the electrical and geometrical parameters of the
four-shelled yeast cell model.

Region	Thickness/ Radius (µm)	Relative Permittivity	Conductivity (S/m)
Cytoplasm	−/2.5	53	1
Membrane	0.008/2.508	5	10^{-7}
Inner Wall	0.2/2.708	60	0.012
Outer Wall	0.05/2.758	6.2	0.021
Suspending Medium	−	80	0.001/ 0.01/0.1

value from the experimental image analysis of the electrorotation of the yeast. The neck radius of the bud was kept constant from 0% start to 100% stage with a value of $R_{neck} = 0.517\,\mu m$ [34]. In Table 1 we show the final values for the electrical and geometrical parameters of the four-shelled yeast cell model that best fit the experimental rotational data. The resulting capacitance and conductance per unit area of the membrane are $C_m = 5.53\,mF/m^2$ and $G_m = 12.5\,S/m^2$ respectively that are within the range of values available in literature [49].

Figure 4 shows the real and imaginary parts of the polarizability of the four-shelled yeast model with the parameters of Table 1, as a function of the frequency. The values are shown for both horizontal and vertical orientations of the external electric field and for σ_{ext} values of 0.001, 0.01 and 0.1 S/m. We observe that the amplitude values of both $Re(\tilde{\alpha}_{eff})$ and $Im(\tilde{\alpha}_{eff})$ decrease as the conductivity increases whereas for horizontal polarization at a given value σ_{ext}, they monotonically increase as the yeast goes from 0% to 100% full division. This behavior is also observed for higher conductivities of the host medium. This is expected as the induced dipoles in both mother and bud are parallel. However, for vertical polarization the induced dipoles are collinear, with a greater mutual interaction and thus with significant changes in the $Im(\tilde{\alpha}_{eff})$ for the doublet cell at the end of the cell cycle (100%).
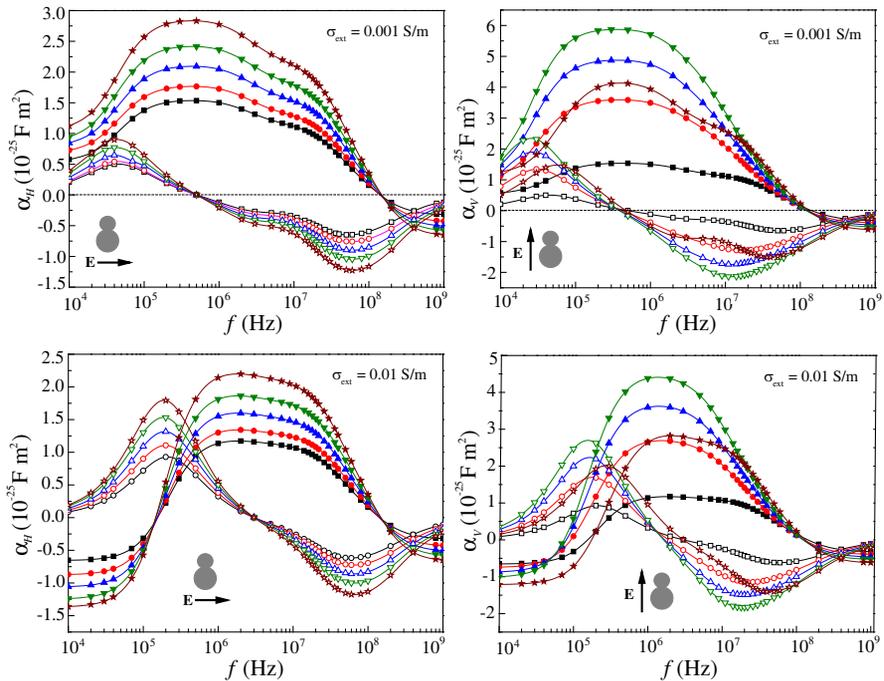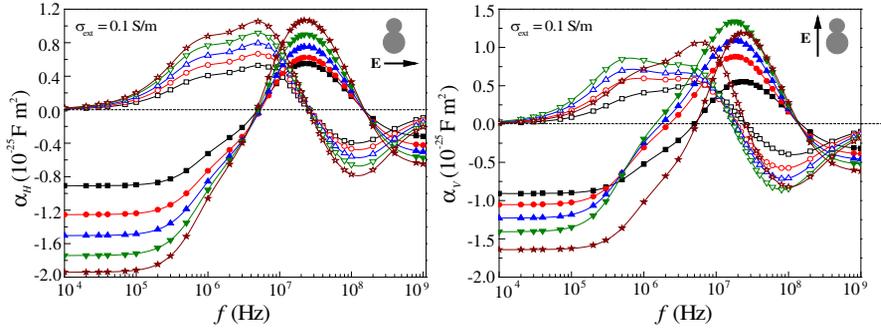
Figure 4. Real (solid markers) and imaginary (empty markers) parts of the horizontal (H) and vertical (V) effective complex polarizability $\tilde{\alpha}_{eff\,H,V}$ of the yeast model described in Section 2 as a function of the frequency f for 0% (square), 25% (circle), 50% (up triangle), 75% (down triangle) and 100% (star) budding states for different values of the host medium conductivity.

Figures 5(a) and 5(b) show the results for the torque spectra of the yeast $N\,(f)$ at 0% budding state for the three characteristic values of σ_{ext} considered above and of the equivalent homogeneous sphere, for a conductivity $\sigma_{\text{ext}} = 0.1\,\text{S/m}$ respectively. A comparison between the torque spectra of Figs. 5(a) and 5(b) for $\sigma_{\text{ext}} = 0.1\,\text{S/m}$, shows that our numerical computation of $\tilde{\alpha}_{eff}$ agrees with the results given by the equivalent permittivity model with a relative error of less than 10^{-5}. The results for the complex permittivity spectra of the equivalent homogeneous sphere, for a conductivity $\sigma_{\text{ext}} = 0.1\,\text{S/m}$, are shown in Fig. 6.

Figure 7 shows the fitting to experimental data of the calculated spectra for the two representative budding states 0% and 50% with host medium conductivities $\sigma_{\text{ext}} = 0.01\,\text{S/m}$ and $\sigma_{\text{ext}} = 0.001\,\text{S/m}$ respectively. For the 0% spectra (spherical yeast), we find that the best fit is obtained for $F = 5.782 \times 10^{14}\,\text{N}^{-1}\text{m}^{-1}\text{s}^{-1}$ which corresponds to a value of $\eta = 1.64\,\text{Pa·s}$ for the suspending medium viscosity. This value is higher than the typical value $\eta \approx 1\,\text{Pa·s}$ of the saline solution used in the experimental chamber [50]. This effective higher viscosity value is reasonable and may be explained by the influence of the proximity of the electrode base plane on the rotation of the yeast confined within the chamber.

As for the 50% yeast budding state, we use the complex polarizability for both orientations shown in Fig. 4 for $\sigma_{\text{ext}} = 0.001\,\text{S/m}$ and use Eq. (4) with the adjustable parameter F to find the best fitting to the experimental ER data. Because of the
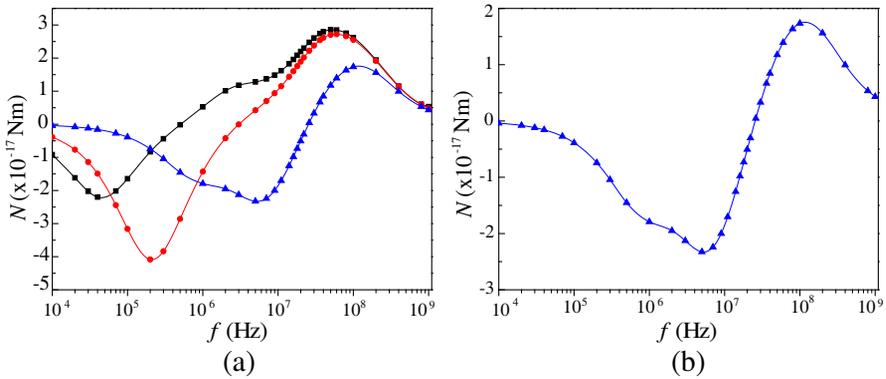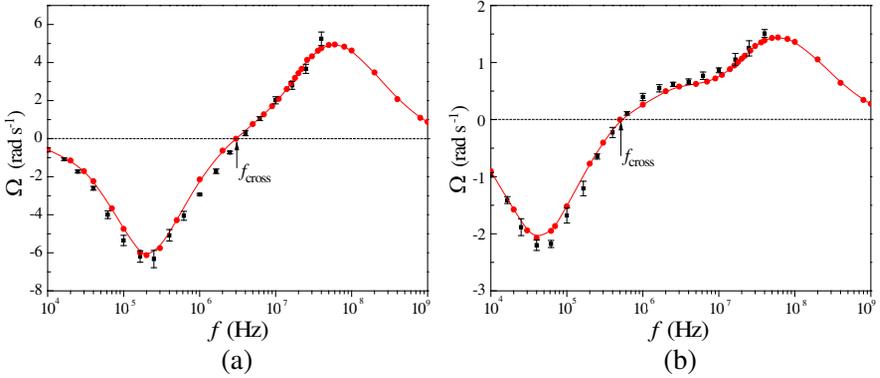
Figure 5. Torque spectra as a function of the frequency f for (a) four-shelled yeast model for $\sigma_{\text{ext}} = 0.001$ (square), 0.01 (circle) and 0.1 S/m (up triangle) and (b) equivalent homogeneous spherical model for $\sigma_{\text{ext}} = 0.1$ S/m.
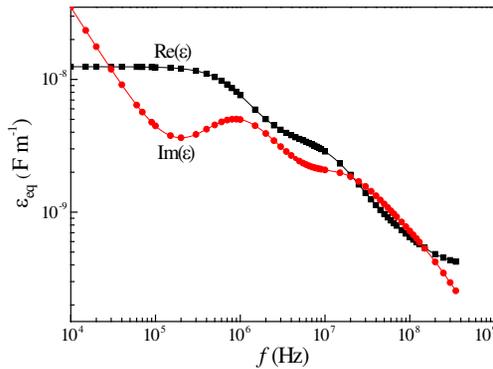

Figure 6. Real part and imaginary parts of the complex permittivity of the equivalent homogeneous spherical model as a function of the frequency f for $\sigma_{\text{ext}} = 0.1$ S/m.

complex geometry of the doublet-shape yeast, no analytical expression is available for parameter F. As a simple approach, we could have used the already available expressions of F for either a multilayered sphere or ellipsoid. However, numerical analysis of the influence of experimental conditions on the accuracy of dielectric parameters derived from electrorotation measurements [51] shows that use of idealized model as deviations from actual particle shapes will lead to inaccuracies in the derived parameters. For the fitting shown in Fig. 7(b) the adjustable parameter has a value of $F = 2.247 \times 10^{15} \, \text{N}^{-1}\text{m}^{-1}\text{s}^{-1}$.

Figure 7. Experimental (square) and calculated (circles) rotation velocity spectra of the yeast as a function of the frequency f, (a) 0% (start) budding state and $\sigma_{\text{ext}} = 0.01\,\text{S/m}$ and (b) 50% budding state and $\sigma_{\text{ext}} = 0.001\,\text{S/m}$.
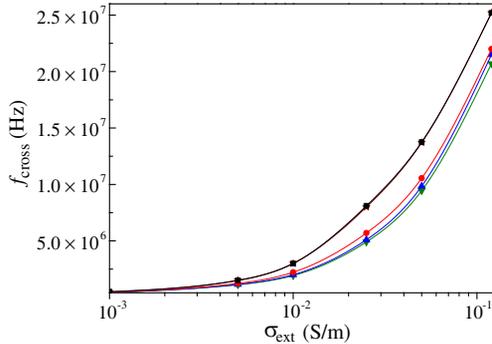
Figure 8. Crossover frequencies of the yeast as a function of the conductivity of the suspending medium for the complete budding yeast cell cycle. Square, circle, up triangle, down triangle and star symbols correspond to 0%, 25%, 50%, 75% and 100% budding states respectively.

The crossover frequency has been frequently used as a convenient parameter to quantify ER behavior. For this reason we have computed the crossover frequency f_{cross} for different budding states as a function of the conductivity of the suspending medium. From the results shown in Fig. 8, we note that for each state, f_{cross} varies almost exponentially with σ_{ext}, whereas for a fixed value of the conductivity, the decrease of the crossover frequency is not significant as the size of the daughter bud grows. Finally, when the daughter bud reaches the size of the

mother cell (100%), the frequency crossover jumps back to the 0% value and the corresponding markers and curves appear to be almost superimposed. The small variation of $f_{\rm cross}$ within a full span of the growth cycle shown in Fig. 8 indicates that the usefulness of this parameter measurement to determine with certainty the yeast budding state may be limited and that a complete spectrum determination is needed.

3.1. Synchronized Solutions

As a further application of the above characterization of the budding yeast, we have used Maxwell-Wagner formalism to obtain the dielectric spectra of synchronized suspensions of yeasts at different budding states. The effective Clausius-Mossotti factor of suspensions in which the particles of volume $V_{\rm cell}$ are randomly oriented is given by [11, 52]

$$\frac{\tilde{\varepsilon}_{sus} - \tilde{\varepsilon}_{\rm ext}}{\tilde{\varepsilon}_{sus} + 2\tilde{\varepsilon}_{\rm ext}} = \frac{P}{9K}(2\tilde{\alpha}_{eff H} + \tilde{\alpha}_{eff V}) \qquad (9)$$

where P is the volume fraction of the particles and $K = \varepsilon_0 \mathrm{Re}(\tilde{\varepsilon}_{\rm ext}) V_{\rm cell}$. To obtain the complex permittivity $\tilde{\varepsilon}_{sus}$ as a function of P, we refer back to Eq. (1) with the cell values of Table 1 to determine the complex polarizabilities $\tilde{\alpha}_{eff H,V}$, the doublet-shaped cell volume $V_{\rm cell}$ and parameter K for different stages of the cell budding cycle. The latter values are shown in Table 2.

Figures 9(a) and 9(b) show the calculated real and imaginary parts of $\tilde{\varepsilon}_{sus}$ of synchronized solutions of yeast cells at 0% and 50% budding states with volume fraction $P = 0.1$, calculated as a function of the frequency f for the conductivity values 0.001, 0.01 and 0.1 S/m of the host medium.

A comparison of Figs. 9(a) and 9(b) shows that, for the same volume concentration and conductivity of the suspending media, an

Table 2. Calculated values of the cell volume $V_{\rm cell}$ and K for the complete yeast budding cycle.

Budding	$V_{\rm cell}$ (m^3)	K
0%	8.787×10^{-17}	6.222×10^{-26}
25%	1.122×10^{-16}	7.944×10^{-26}
50%	1.335×10^{-16}	9.452×10^{-26}
75%	1.538×10^{-16}	1.089×10^{-25}
100%	1.757×10^{-16}	1.244×10^{-25}
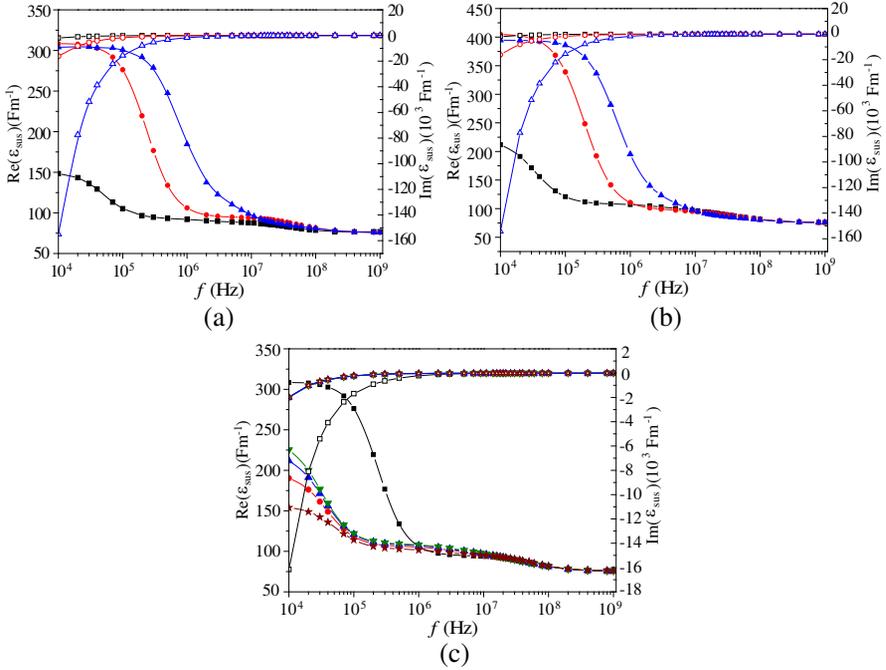
Figure 9. Frequency dependence of the real (solid markers) and imaginary parts (empty markers) of the complex permittivity of (a) 0% and (b) 50% yeast budding synchronized suspensions for values $\sigma_{\text{ext}} = 0.001\,\text{S/m}$ (square), $\sigma_{\text{ext}} = 0.01\,\text{S/m}$ (circle) and $\sigma_{\text{ext}} = 0.1\,\text{S/m}$ (up triangle). Fig. 9(c) shows the complex permittivity of 0% (square), 25% (circle), 50% (up triangle), 75% (down triangle) and 100% (star) yeast budding synchronized suspensions for a host medium conductivity value of $\sigma_{\text{ext}} = 0.001$ S/m. The fraction volume is $P = 0.1$.

active yeast budding process leads to a significant change in the real part of the permittivity of the suspension, whereas changes in the imaginary part are less noticeable except for the highest value of the host medium conductivity. This is also clearly observed in Fig. 9(c), that shows the real and imaginary parts of the permittivity of synchronized suspensions for the full budding cycle and for constant values of $P = 0.1$ and $\sigma_{\text{ext}} = 0.001\,\text{S/m}$. This study shows that the cell shape change of suspending particles from the single-cell to doublet-cell affects the frequency dependence of permittivity ε and conductivity σ, and therefore the behavior of doublet-shaped particles cannot be simulated by spheroidal models [9, 53].

4. CONCLUSIONS

In this paper, we have electrically characterized the *S. cerevisiae* budding cell cycle from both experimental and theoretical points of view and we have combined these two approaches to obtain the electrical parameters for every compartment of the yeast as well as a better knowledge of the budding state within the cell cycle. For this task, we have designed the experimental electrorotation chamber and associated electronics to determine the rotational velocity spectra of single yeasts at different stages of the budding cycle and environmental conditions. Then we have used a numerical technique based on finite element to electrically simulate the actual ER chamber filled with the same suspending medium, the phase shifted voltage signals and four electrodes chip to determine the field distribution within the chamber. We have focused our interest on the square of the electric field to derive the first order dipolar torque acting on the cell. A four-shelled structure based on electron micrographs was used for the yeast, with spherical and doublet-shaped geometrical models for start and different budding states respectively.

To calculate the torque and the rotational velocity spectra we first determine the particle complex polarizability by using a technique based on a weighted average of the dielectric polarization, which has the advantage of being applicable to any geometrical shape (spherical or doublet shaped) of the yeast. In order to check our results we also consider a homogeneous spherical yeast with same radius as the outer wall of our multilayer yeast model and with an equivalent complex permittivity.

To derive the geometrical and electrical parameters of our yeast model we use an iterative process and apply the least-square method to fit the numerical rotational velocity spectrum to experimental data. For fitting the spectra to data for the spherical and doublet-shaped models, we use as adjustable parameters the viscosity of the suspending medium and a form factor respectively.

We have shown that the calculated yeast ER spectra undergo significant changes throughout its budding cycle and that the calculated spectra fit experimental data obtained for 0% (start) and 50% representative budding stages for different conductivities of the host medium very well. The fitting results provide the geometrical and electrical parameters of our realistic yeast model. The analysis also shows how the small variation of the rotation crossover frequency within a full span of the yeast growth cycle does not provide reliable information on the budding state of the yeast.

Finally, we have applied the well-known Maxwell-Wagner

formalism to obtain the dielectric spectra of truly synchronized suspensions. We note that the observed changes in the complex permittivity of the solution are mainly due to the shape modifications, from single-cells to doublet-cells, experienced by the yeast throughout the budding cycle.

ACKNOWLEDGMENT

REFERENCES

1. MacQueen, L. A., M. Thibault, M. D. Buschmann, and M. R. Wertheimer, "Electro-manipulation of biological cells in microdevices," *IEEE Transactions on Dielectrics and Electrical Insulation*, Vol. 19, No. 4, 1261–1268, 2012.

2. Li, H., T. Ye, and K. Y. Lam, "Numerical modeling of motion trajectory and deformation behavior of a cell in a nonuniform electric field," *Biomicrofluidics*, Vol. 5, 021101, 2011.

3. Jones, T. B., "Basic theory of dielectrophoresis and electrorotation," *IEEE Engineering in Medicine and Biology Magazine*, 33–42, 2003.

4. Cena, E. G., C. Daltona, Y. Lia, S. Adamiab, L. M. Pilarskib, and K. V. I. S. Kaler, "A combined dielectrophoresis, traveling wave dielectrophoresis and electrorotation microchip for the manipulation and characterization of human malignant cells," *Journal of Microbiological Methods*, Vol. 58, 387–401, 2004.

5. Sancho, M., G. Martínez, S. Muñoz, J. L. Sebastián, and R. Pethig, "Interaction between cells in dielectrophoresis and electrorotation experiments," *Biomicrofluidics*, Vol. 4, 022802, 2010.

6. Hoettges, K. F., "Dielectrophoresis as a cell characterisation tool," *Microengineering in Biotechnology: Methods in Molecular Biology*, Vol, 583, 183–198, 2008.

7. Zienkiewicz, O. C., *The Finite Element Method*, 3rd Edition, McGraw-Hill, London, 1977.

8. Johnson, C., *Numerical Solutions of Partial Differential Equations*

by the Finite Element Method, Cambridge University Press, Cambridge, 1987.

9. Sekine, K., "Application of boundary element method to calculation of the complex permittivity of suspensions of cells in shape of D∞h symmetry," *Bioelectrochemistry*, Vol. 52, 1–7, 2000.

10. Sancho, M., G. Martinez, and C. Martin, "Accurate dielectric modeling of shelled particles and cells," *J. Electrost.*, Vol. 57, 143–156, 2003.

11. Sekine, K., Y. Watanabe, S. Hara, and K. Asami, "Boundary-element calculations for dielectric behavior of doublet-shaped cells," *Biochim. Biophys. Acta*, Vol. 1721, 130–138, 2005.

12. Pruyne, D., A. Legesse-Miller, L. Gao, Y. Dong, and A. Bretscher, "Mechanisms of polarized growth and organelle segregation in yeast," *Annu. Rev. Cell Dev. Biol.*, Vol. 20, 559–591, 2004.

13. McMurray, M. A. and J. Thorner, "Septins: Molecular partitioning and the generation of cellular asymmetry," *Cell Division*, Vol. 4, 18, 2009.

14. Held, P., "Monitoring growth of beer brewing strains of saccharomyces cerevisiae — The utility of synergy H1 for providing high quality kinetic data for yeast growth applications," Biotek Application Note, 2010.

15. Asami, K., "Characterization of biological cells by dielectric spectroscopy," *Journal of Non-Crystalline Solids*, Vol. 305, 268–277, 2002.

16. Asami, K. and T. Yonezawa, "Dielectric behavior of non-spherical cells in culture," *Biochim. Biophys. Acta*, Vol. 1245, 317–324, 1995.

17. Asami, K., E. Gheorghiu, and T. Yonezawa, "Dielectric behavior of budding yeast in cell separation," *Biochim. Biophys. Acta*, Vol. 1381, 234–240, 1998.

18. Lei, J., J. T. K. Wan, K. W. Yu, and H. Sun, "Dielectric behavior of nonspherical cell suspensions," *J. Phys.: Condens. Matter*, Vol. 13, 3583–3589, 2001.

19. Bordi, F., C. Cametti, and T. Gili, "Dielectric spectroscopy of erythrocyte cell suspensions. A comparison between Looyenga and Maxwell-Wagner-Hanai effective medium theory formulations," *Journal of Non-Crystalline Solids*, Vol. 305, 278–284, 2002.

20. Adohi, B. J-P., C. V. Bouanga, K. Fatyeyeva, and M. Tabellout, "Application of the Maxwell-Wagner-Hanai effective medium theory to the analysis of the interfacial polarization relaxations in conducting composite films," *J. Phys. D: Appl. Phys.*, Vol. 42,

015302, 2009.

21. Di Biasio, A., L. Ambrosonne, and C. Cametti, "The dielectric behavior of nonspherical biological cell suspensions: An analytical approach," *Biophys. J.*, Vol. 99, 163–174, 2010.

22. Asami, K., "Dielectric dispersion in biological cells of complex geometry simulated by the three-dimensional finite difference method," *J. Phys. D: Appl. Phys.*, Vol. 39, 492–499, 2006.

23. Hözel, R., "Electric field calculation for electrorotation electrodes," *J. Phys. D: Appl. Phys.*, Vol. 26, 2112–2116, 1993.

24. Maswiwat, K., M. Holtappels, and J. Gimsa, "Optimizing the electrode shape for four-electrode electrorotation chips," *ScienceAsia*, Vol. 33, 61–67, 2007.

25. Maswiwat, K., M. Holtappels, and J. Gimsa, "On the field distribution in electrorotation chambers: Influence of electrode shape," *Electrochimica Acta*, Vol. 51, No. 24, 5215–5220, 2006.

26. Kakutani, T., S. Shibatani, and M. Sugai, "Electrorotation of non-spherical cells: Theory for ellipsoildal cells with an arbitrary number of shells," *Bioelectrochemistry and Bioenergetics*, Vol. 31, 131–145, 1993.

27. Laforet, J., M. Frenea-Robin, H. Ceremonie, F. Buret, and L. Nicolas, "Automated cell characterization platform: Application to yeast protoplast study by electrorotation," *Proc. of the 1st Int. Conf. on Biomedical Electronics and Devices, Biodevices*, Funchal, Portugal, 2008, ISBN:978-989-8111-17-3.

28. Hughes, M. P., "Computer-aided analysis of conditions for optimizing practical electrorotation," *Phys. Med. Biol.*, Vol. 43, 3639–3648, 1998.

29. Hughes, M. P., X. B. Wang, F. F. Becker, P. R. C. Gascoyne, and R. Pethig, "Computer-aided analyses of electric fields used in electrorotation studies," *J. Phys. D: Appl. Phys.*, Vol. 27, 1564–1570, 1994.

30. Hözel, R., "Electrorotation of single yeast cells at frequencies between 100 Hz and 1.6 GHz," *Biophys. J.*, Vol. 73, No. 2, 1103–1109, 1997.

31. Vitols, E., R. J. North, and A. W. Linnane, "Studies on the oxidative metabolism of Saccharomyces cerevisiae. I. Observations on the fine structure of the yeast cell," *J. Biophys. Biochem. Cytol.*, Vol. 9, 689–699, 1961.

32. Moore, C. W., R. del Valle, J. McKoy, A. Pramanik, and R. E. Gordon, "Lesions and preferential initial localization of [S-methyl-3H] bleomycin A2 on Saccharomyces cerevisiae cell walls

and membranes," *Antimicrob. Agents Chemother.*, Vol. 36, No. 11, 2497–2505, 1992.

33. Mulholland, J., D. Preuss, A. Moon, A. Wong, D. Dubrin, and D. Botstein, "Ultrastructure of the yeast actin cytoskeleton and its association," *The Journal of Cell Biology*, Vol. 125, No. 2, 381–391, 1994.

34. Asami, K. and K. Sekine, "Dielectric modelling of cell division for budding and fission yeast," *J. Phys. D: Appl. Phys.*, Vol. 40, 1128–1133, 2007.

35. Sebastián, J. L., S. Muñoz, M. Sancho, G. Martínez, and G. Alvarez, "Electromechanical effects on multilayered cells in nonuniform rotating fields," *Physical Review E*, Vol. 84, 011926, 2011.

36. Sebastián, J. L., S. Muñoz, M. Sancho, and G. Alvarez, "Polarizability of shelled particles of arbitrary shape in lossy media with an application to hematic cells," *Physical Review E*, Vol. 78, 051905, 2008.

37. Wang, X. B., R. Pethig, and T. B. Jones, "Relationship of dielectrophoretic and electrorotational behaviour exhibited by polarized particles," *J. Phys. D: Appl. Phys.*, Vol. 25, 905–912, 1992.

38. Wang, X. B., Y. Huang, R. Holzel, J. P. H. Burt, and R. Pethig, "Theoretical and experimental investigations of the interdependence of the dielectric, dielectrophoretic and electrorotational behavior of colloidal particles," *J. Phys. D: Appl. Phys.*, Vol. 26, 312–322, 1993.

39. Jones, T. B., *Electromechanics of Particles*, Cambridge University Press, Cambridge, 1995.

40. Wang, X. J., X. B. Wang, and P. R. C. Gascoyne, "General expressions for dielectrophoretic force and electrorotational torque derived using the Maxwell stress tensor method," *J. Electrost.*, Vol. 39, 277–296, 1997.

41. Huang, Y., R. Hölzel, R. Pethig, and X. B. Wang, "Differences in the AC electrodynamics of viable and non-viable yeast cells determined through combined dielectrophoresis and electrorotation studies," *Phys. Med. Biol.*, Vol. 37, No. 7, 1499–1517, 1992.

42. Huang, J. P. and K. W. Yu, "First-principles approach to electrorotation assay," *J. Phys.: Condens. Matter*, Vol. 14, 1213–1221, 2002.

43. Kriegmaier, M., M. Zimmermann, K. Wolf, U. Zimmermann, and V. L. Sukhorukov, "Dielectric spectroscopy of Schizosac-

charomyces pombe using electrorotation and electroorientation," *Biochim. Biophys. Acta*, Vol. 1568, 135–146, 2001.

44. Misirli, Z., E. T. Oner, and B. Kirdar, "Real imaging and size values of Saccharomyces cerevisiae cells with comparable contrast tuning to two environmental scanning electron microscopy modes," *Scanning*, Vol. 29, No. 1, 11–19, 2007.

45. Ren, Y., A. M. Donald, and Z. Zhang, "Investigation of the morphology, viability and mechanical properties of yeast cells in environmental SEM," *Scanning*, Vol. 30, No. 6, 435–442, 2008.

46. Osumi, M., "The ultrastructure of yeast: Cell structure and wall formation," *Micron.*, Vol. 29, No. 2–3, 207–233, 1998.

47. Lesage, G. and H. Bussey, "Cell wall assembly in saccharomyces cerevisiae," *Microbiol. Mol. Biol. Rev.*, Vol. 70, No. 2, 317–343, 2006.

48. Ferrier, G. A., A. N. Hladio, D. J. Thomson, G. E. Bridges, M. Hedayatipoor, S. Olson, and M. R. Freeman, "Microfluidic electromanipulation with capacitive detection for the mechanical analysis of cells," *Biomicrofluidics*, Vol. 2, 044102 (13 pages), 2008.

49. Christopher, L. D., H. M. Gerard, and B. K. Douglas, "On the dielectric method of monitoring cellular viability," *Pure & App. Chern.*, Vol. 65, No. 9, 1921–1926, 1993.

50. Kestin, J., H. E. Khalifa, and R. J. Correia, "Tables of the dynamic and kinematic viscosity of aqueous NaCl solutions in the temperature range 20–150°C and the pressure range 0.1–35 MPa," *J. Phys. Chem. Ref. Data*, Vol. 10, No. 1, 1981.

51. Gascoyne, P. R. C., F. F. Becker, and X. B. Wang, "Numerical analysis of the influence of experimental conditions on the accuracy of dielectric parameters derived from electrorotation measurements," *Bioelectrochemistry and Bioenergetics*, Vol. 36, 115–125, 1995.

52. Gimsa, J. and D. Wachner, "A polarization model overcoming the geometric restrictions of the Laplace solution for spheroidal cells: Obtaining new equations for field induced forces and transmembrane potential," *Biophys. J.*, Vol. 77, 1316–1326, 1999.

53. Asami, K., E. Gheorghiu, and T. Yonezawa, "Dielectric behavior of budding yeast in cell separation," *Biochim. Biophys. Acta*, Vol. 1381, 234–240, 1998.